Talanta 85 (2011) 469–475

Contents lists available at ScienceDirect

Talanta

journal homepage: www.elsevier.com/locate/talanta

3-Aminopropyltriethoxysilane-functionalized manganese doped ZnS quantum dots for room-temperature phosphorescence sensing ultratrace 2,4,6-trinitrotoluene in aqueous solution

Ya-qin Wang, Wen-sheng Zou*

School of Materials and Chemical Engineering, Anhui University of Architecture, 856 South Jinzhai Road, Hefei 230022, PR China

ARTICLE INFO

Article history:
Received 10 December 2010
Received in revised form 30 March 2011
Accepted 5 April 2011
Available online 12 April 2011

Keywords:
3-Aminopropyltriethoxysilane (APTES)
Mn doped ZnS QDs
2,4,6-Trinitrotoluene (TNT)
Acid–base pairing interaction
Room-temperature phosphorescence (RTP)

ABSTRACT

New strategies for silica coating of inorganic nanoparticles became a research hotspot for enhancing the mechanical stability of colloidal particles and protecting colloidal particles against oxidation and agglomeration, and so on. In this paper, 3-aminopropyltriethoxysilane (APTES)-functionalized Mn doped (AF MnD) ZnS QDs was prepared to be firsyly through the use of silane coupling agents to form an active layer of silica, then sol–gel reaction of TEOS co-deposited with APTES on the surface of resultant active layer of silica. The emitted long lifetime room-temperature phosphorescence (RTP) of the resultant nanomaterials allows an appropriate delay time so that any fluorescent emission and scattering light can be easily avoided. The APTES anchored on the layer of silica can bind 2,4,6-trinitrotoluene (TNT) species to form TNT anion through acid–base pairing interaction, the TNT anion species may increase the charge-transfer pathways from the nanocrystals to nitroaromatic analytes, therefore further enhance the quenching efficiency of RTP. Moreover, APTES as capped reagents can enlarge the spectral sensitivity and enhance RTP response of nanocrystals to the electron-deficient nitroaromatic and nitrophenol species. Meanwhile, AF MnD ZnS QDs also exhibited a highly selective response toward TNT analyte through significant color change and quenching of $^4T_1$ to $^6A_1$ transition emission. This AF MnD ZnS QDs based sensor showed a very good linearity in the range of 0.05–1.8 μM with detection limit down to 50 nM (quenching percentage of phosphorescence intensity of 8%) and RSD of 3.5% (n = 5). The reported QDs-based chemosensors here open up a promising prospect for the sensitive and convenient sensing of TNT explosive.

1. Introduction

In recent years, new strategies for silica coating of nanomaterials, different from the classical methodologies, have emerged at the forefront of materials science [1,2]. At least three classical technologies such as Stöber synthesis [3,4], use of silane coupling agents [5], and the sodium silicate water-glass methodology [6,7] have been devoted to silica coating of colloidal nanoparticles by classical aqueous methods. Although many different approaches have, so far, been developed for the synthesis of nanoparticles with core@SiO_2 geometries, the majority of them are based on the above-mentioned methods. Silica as a coating material by using core–shell rational designs and its synthetic versatility holds an unparalleled advantages for enhancing the mechanical stability of colloidal particles, enabling a transfer into various organic and aqueous solvents, and protecting colloidal particles against oxidation and agglomeration. Moreover, the nanomaterials coated with a silica shell would be highly desirable to impart biocompatibility with biological assays [8–10], and semiconductor QDs deposited with a silica shell would be helpful to reduce cytotoxicity [11] and use for assembly of photonic structures [12], and so on. Recently, because the interference from auto-fluorescence emission and scattering light can be easily avoided due to the long lifetime of phosphorescence [13], room-temperature phosphorescence (RTP) has been studied in a number of doped semiconductor systems [14–18]. Tu et al. [19] synthesized amine-capped MnD ZnS nanocrystals and used it in the field of analysis for the first time. Subsequently, Yan's group applied such nanocrystals in RTP sensing DNA [20], persistent organic pollutants (POPs) in water [21], enoxacin [22] and glucose [23] in biological fluids. More recently, we have also reported a Rayleigh scattering chemodosimeter and RTP chemosensor dual recognition probe for the detection of TNT based on L-cysteine capped Mn doped ZnS QDs [24].

Here, we reported the synthesis of 3-aminopropyltriethoxysilane (APTES)-functionalized Mn doped (AF MnD) ZnS QDs with unusual 2,4,6-trinitrotoluene (TNT) recognition

* Corresponding author. Tel.: +86 551 3828 150.
E-mail address: wshzou@yahoo.cn (W.-s. Zou).

0039-9140/$ – see front matter © 2011 Elsevier B.V. All rights reserved.
doi:10.1016/j.talanta.2011.04.014

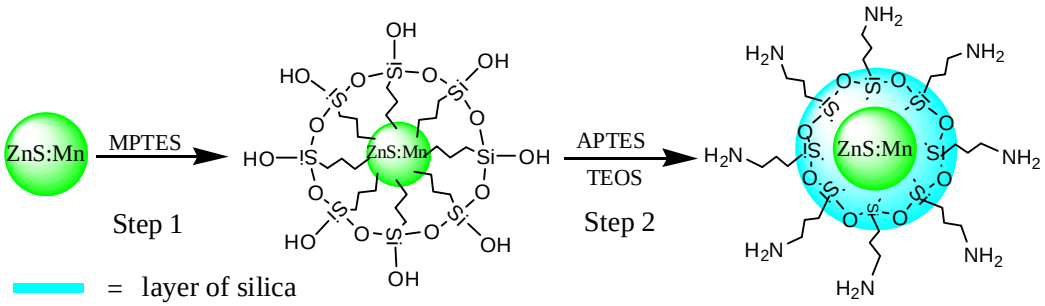

Fig. 1. Schematic illustration for the preparation of AF MnD ZnS QDs.

function and the study of its RTP sensing feature. The AF MnD ZnS QDs can bind TNT species to form TNT anion through acid–base pairing interaction between electron-rich amino ligands and electron-deficient aromatic rings [19]. Generally, TNT anion may quench fluorescence of the QDs with the band gap close to the absorption edge of TNT through a charge-transfer process [25]. Therefore dramatic RTP reduction at $^4T_1$ to $^6A_1$ transition emission wavelength was observed. Notably, AF MnD ZnS QDs also exhibited a highly selective response toward TNT analyte through significant color change.

TNT has always been magnetizing tremendous societal concern due to TNT not only as notorious high explosive menacing societal security but also as significant deleterious species influencing environment and human health [26,27]. In recent decade, since QDs offer advantages over conventional organic fluorophores such as great photostability, size-dependent emission wavelengths or the introduction of dopant ions, and sharp emission profile, which can be utilized as chemosensor to provide the chemodetection selectivity and sensitivity to target species [19,28]. Recently, ligands containing lone-electron pair capped gold nanoparticles exhibited high surface enhanced Raman spectroscopy (SERS) response [29] and colorimetric sensitivity [30] for TNT at picomolar levels. Molecular imprinted (MI) technique, a way to change or fine-tune the chemodetection selectivity, utilized molecular shape of a target analyte as a natural feature to enhance molecular recognition. This versatile approach has been used to create affinity in solid matrices for TNT through controlled selection of functional groups location and shape recognition [31]. The above approaches have led to significant contributions to the TNT assay. Under the guide of the faith of low-carbon life and green environment, and the attraction of nanomaterials' excellent properties, it is still desirable to develop new nanoparticles-based methods with the feature of cost-effectiveness, easy-to-operation, procedure simplicity, time-saving or environment-friendliness. Such approach requires the integration of simple and green synthetical technique, selective recognition and highly sensitive detectable signals, etc. The proposed methods are well-suited for detecting the ultra-trace TNT and distinguishing different nitro compounds in aqueous solution.

2. Experimental

2.1. Chemicals

2,4,6-Trinitrotoluene (TNT), 2,4-dinitrotoluene (DNT) and 4-nitrotoluene (NT) were gifted friendly by Professor Zhao-Wu Shen (University of Science and Technology of China, Hefei, Anhui, China) and used as recrystallized from methanol–water (2:1, v/v) mixture. 4-nitrophenol (4-NP) with a purity of over 99.5%, fulvic acid with carbon content over 40% and tetraethoxysilane (TEOS) with a purity of over 99% were commercially purchased from Sinopharm Chemical Reagent Co., Ltd. (Shanghai, China). 3-Aminopropyltriethoxysilane (APTES, purity > 98%) and 3-mercaptopropyltriethoxysilane (MPTS, purity > 99%) were the products of Alfa Aesar (Tianjin, China) and Aladdin (Shanghai, China), respectively. $ZnSO_4{\cdot}7H_2O$, $Na_2S{\cdot}9H_2O$ and $MnCl_2{\cdot}4H_2O$ were purchased and used as received. The stock solutions of TNT, DNT, NT and 4-NP were prepared by dissolving in ethanol with concentration of 2×10^{-3} M for TNT, and 2×10^{-2} M for others, as used they were diluted to desired concentration. The concentration of Mn-doped ZnS QDs was 400 mg/L. Doubly deionized water (DDW) was prepared in Elix 5 pure water system (Millipore, Milwood, MA, USA). All other reagents were of analytical grade and used without further purification.

2.2. Synthesis of the AF MnD ZnS QDs

A two-step preparation procedure was adopted to prepare AF MnD ZnS QDs (Fig. 1) according to the reported procedure with slight modifications [19]. In the first step, 6.25 mmol of 1.8 g $ZnSO_4{\cdot}7H_2O$, 0.5 mmol of 0.1 g $MnCl_2{\cdot}4H_2O$, and 20 mL of DDW were added to a three-necked flask. After the mixture was stirred under dry nitrogen at room temperature for 10 min, 5 mL of aqueous solution containing 6.25 mmol of 1.5 g $Na_2S{\cdot}4H_2O$ was added dropwise, and the mixture was kept stirring for 30 min. Then 5 mL of an ethanol solution containing 0.3 mmol of 0.072 g MPTS was added, and the mixture was kept stirring for 24 h. The resultant MPTS capped Mn doped ZnS QDs were centrifuged and washed with DDW and absolute ethanol three times and dried in vacuum. In the second step, 10 mL of an absolute ethanol solution containing 200 μL of APTES and 0.35 mL of TEOS were added to a 25 mL flask, after stirring 10 min, 0.35 mmol of 250 mg MPTS capped Mn doped ZnS QDs, 0.4 mL of 25% $NH_3{\cdot}H_2O$ and 2.0 mL H_2O were added and stirred for 18 h. Another type of QDs was also synthesized in parallel but without addition of APTES (Mn doped ZnS QDs@SiO_2). The resultant MnD ZnS QDs were centrifuged and washed with 40 mL of absolute ethanol two times to get the QDs with nearly the same RTP intensity. Finally, two types of concentrated MnD ZnS QDs were stored in aqueous solution for convenient operation in experiments.

2.3. Apparatus

UV–vis absorption spectra were obtained using a UV-3600 UV–vis spectrophotometer (Shimadzu, Tokyo, Japan), the RTP and RLS spectra were recorded on an F-4600 (Hitachi, Tokyo, Japan) and the measurements were performed with excitation wavelength at 316 nm equipped with a plotter unit and a quartz cell (1 cm × 1 cm) in a variety of modes. The acidity was measured with a Sartorius PB-10 pH meter (Sartorius, Dietikon, Switzerland). The X-ray diffraction (XRD) spectra were collected on a Shimadzu XRD-6000 diffractometer with Cu Kα radiation. Fourier transform infrared (FT-IR) spectra (4000–400 cm^{-1}) in KBr were recorded on a Nicolet-6700 spectrometer (Nicolet, Madison, WI, USA). The morphology

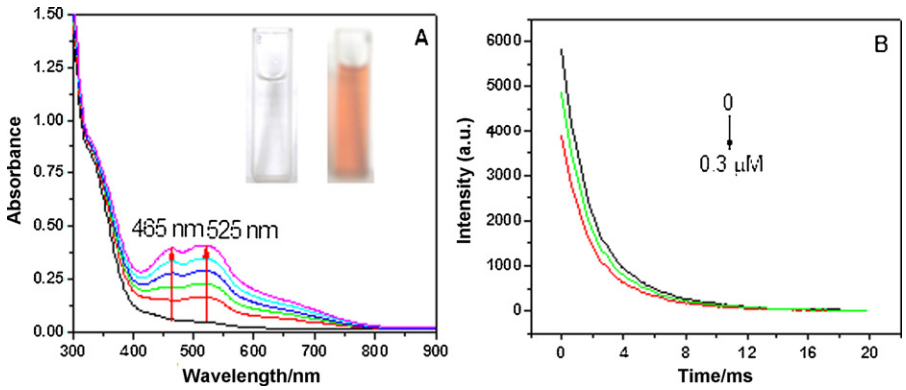

Fig. 2. UV–vis spectra of the TNT (1 mM, 3 mL) anion compounded with APTES (50 μL every time). The Insets show the corresponding colors at different concentration of APTES. Colorless (APTES, 0 μL) and red (APTES, 250 μL) (A). The decay curves of phosphorescence emission of AF MnD ZnS QDs with and without TNT (B).

and microstructure of the QDs were characterized by high resolution transmission electron microscopy (HRTEM) on a JEM-200CX (JEOL, Tokyo, Japan) microscope operating at a 200 kV accelerating voltage. The samples for TEM were obtained by drying sample droplets from water dispersion onto a 300-mesh Cu grid coated with a lacey carbon film, which was then allowed to dry prior to imaging. The mineral ions of real water sample were analyzed by ELAN 9000 ICP-MS (PerkinElmer, USA).

2.4. Spectroscopic measurement

Spectral measurements were carried out with excitation and emission slit width of 10 nm and 20 nm for phosphorescence mode and both of 10 nm for synchronous mode, respectively. Photomultiplier tube voltage, 400 V and 950 V were used for synchronous and phosphorescence, respectively. Phosphorescence at an emission wavelength of 580 nm was monitored at an excitation wavelength at 316 nm, and RLS spectra were recorded by scanning simultaneously the excitation and emission monochromators ($\Delta\lambda = 0$) of the F-4600 spectrophotometer.

2.5. Analysis of water sample

The water samples were collected in a pre-cleaned glass bottle from local rivers and lakes. The samples were filtered through 0.45 μm Supor filters and stored in refrigerator. Because no TNT in the collected water samples was detectable by the proposed method, a recovery test was carried out on the samples spiked with 50, 75 and 100 nM TNT to evaluate its reliability after the pH of filtered water sample was adjusted to 7.5.

3. Results and discussion

3.1. RTP quenching mechanism of AF MnD ZnS QDs

TNT is typically electron-deficient due to the strong electron withdrawing effect of nitro groups, a charge transfer complexing interaction takes place between the electron-deficient aromatic ring of TNT and electron-rich amino group to form TNT anion in solution [32]. The generation of TNT anion can strongly absorb the visible light, leading to the change of solution color (see Inset in Fig. 2A), this phenomenon was firstly observed by Janovsky and Erb in 1886 [33]. TNT anion may quench the emission of the QDs with the band gap close to the absorption band edge of TNT through a charge transfer process [25]. The UV absorption band of the TNT anion is approaching the band gap of the Mn doped ZnS QDs from the absorption spectra of Mn doped ZnS QDs [19]. The charge at the conductive band of the QDs can directly transfer to the LUMO

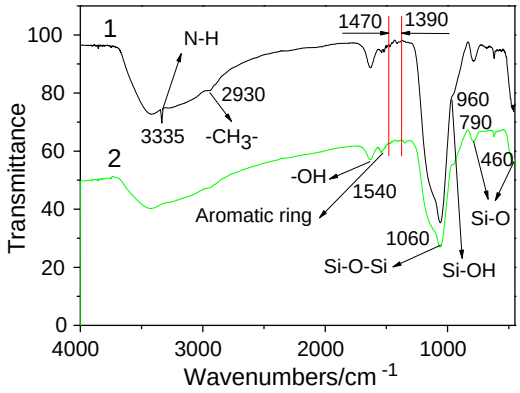

Fig. 3. FT-IR spectra of AF MnD ZnS QDs before (curve 1) and after (curve 2) TNT assembled on its surface.

of the ultraviolet band of the TNT anion. Moreover, because the visible absorption wavelengths of TNT anion (at 465 nm and 525 nm) are much shorter than the emission wavelength of $^4T_1$ to $^6A_1$ transition of Mn^{2+} (at 580 nm) but longer than the emission wavelength of Mn doped ZnS QDs (at 430 nm), the electrons may also transfer from the conductive band and defect band to the LUMO of visible band of the TNT anion. Such mechanism has also been reported by several research groups [19,21,24]. Besides, due to the overall overlap at 580 nm and partial overlap of other absorption bands of TNT anion with the emission of AF MnD ZnS QDs, the fluorescence resonance energy transfer (FRET) also possibly contributed to the quenching of emission of AF MnD ZnS QDs.

To ascertain the interaction between AF MnD ZnS QDs and TNT molecule, FT-IR spectra of AF MnD ZnS QDs before (curve 1) and after (curve 2) TNT assembled on its surface were compared in Fig. 3. The curve 2 displayed clearly the characteristic peaks including the aromatic rings at 1540 cm^{-1} and nitro groups at 1350 cm^{-1}. Compared with the curve 2, curve 1 displayed the characteristic peaks of amino groups at the range of 1390–1470 cm^{-1} [34]. The change of 1390–1470 cm^{-1} band, as well as the disappearance of N–H bent vibration at 3335 cm^{-1} on the curve 2 indicated that the amino group was involved in the formation of the TNT anion [35]. Moreover, such interactions were also investigated by monitoring the phosphorescence emission decay. It is found that in the presence of TNT the phosphorescence intensity of AF MnD ZnS QDs decreased but emission lifetime of AF MnD ZnS QDs did not undergo any evident variation (see Fig. 2B), indicating that TNT led to the formation of anion with AF MnD ZnS QDs without affecting the decay kinetics of radiative and nonradiative processes. Our RLS spectra (see Fig. 6B) also confirmed the formation of anion between AF MnD

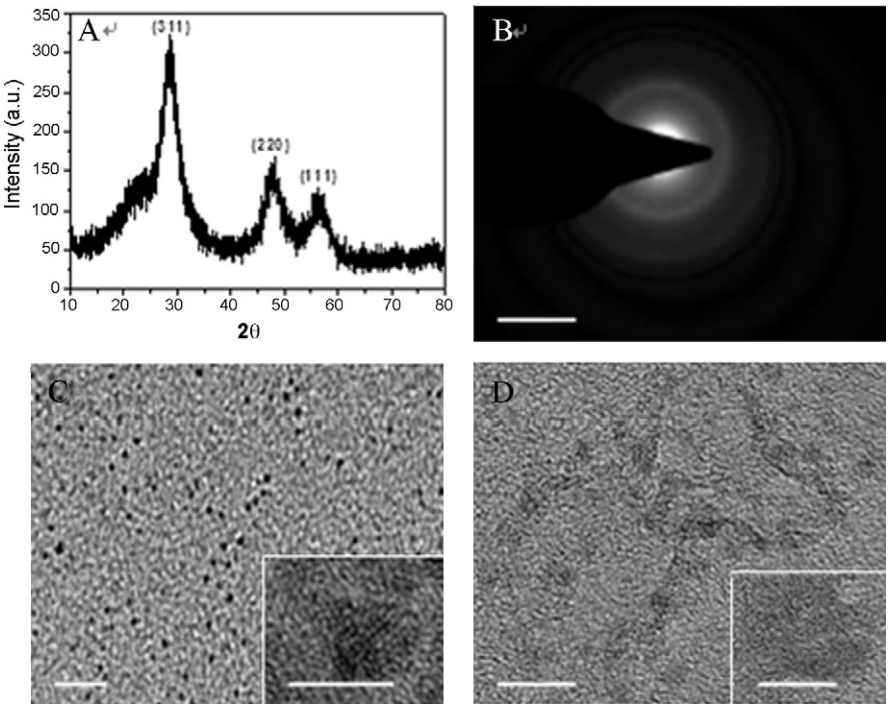

Fig. 4. XRD patterns of MPTS capped MnD ZnS QDs (A). SAED patterns of AF MnD ZnS QDs (B). TEM images of MPTS capped (C) and AF (D) MnD ZnS QDs. HRTEM images of MPTS capped (Inset C) and AF (Inset D) MnD ZnS QDs. Scale bars in B and C, Inset C D and D are 10, 50, 5, 30 and 10 nm, respectively.

ZnS QDs and TNT. As for other nitro aromatic compounds, the lack of nitro group results in the lack of positive charge in benzene ring, which confined the formation of TNT anion.

3.2. Preparation and characterization of the AF MnD ZnS QDs

AF MnD ZnS QDs was prepared through the use of silane coupling agents in the first step. Mercapto groups of MPTS tightly attached onto the surface of the bare Mn doped ZnS nanocrystals and hydroxyl groups of MPTS formed active layer of silica via intermolecular dehydration. Then sol–gel reaction of TEOS co-deposited with APTES on the surface of such active layer of silica. The XRD pattern of AF MnD ZnS QDs exhibited a cubic structure with peaks for (3 1 1), (2 2 0) and (1 1 1) planes (see Fig. 4A). The HRTEM image revealed MPTS capped MnD ZnS QDs with spherical shape and almost uniform size in diameter about 5 nm (see Fig. 4C), which was embedded in a larger particle with the size of ~16 nm as revealed by the TEM images (see Fig. 4D). The selected area electron diffraction (SAED) patterns of the AF MnD ZnS QDs (Fig. 4B) shows the outer diffraction rings of the cubic structure of these AF MnD ZnS QDs polycrystallites. The $-CH_2-$ (~2930 cm^{-1}), strong and broad peak Si–O–Si (~1060 cm^{-1}) and Si–O vibration (789 and 459 cm^{-1}) existing in the FT-IR spectra of MPTS capped MnD ZnS QDs indicated the MPTS covalently interacted onto the surface of nanocrystals through thiols [21]. Moreover, N–H (~3335 and 1390–1470 cm^{-1}) existing in the FT-IR spectra of AF MnD ZnS QDs manifested successful APTES functionalization of MPTS capped MnD ZnS QDs via sol–gel reaction (Fig. 4). The nanocrystals can keep monodispersion but not aggregation for months in aqueous solution.

3.3. Emission characteristics of the AF MnD ZnS QDs

AF MnD ZnS QDs displays bright orange fluorescence in a UV lamp box (see Inset (left) in Fig. 5), suggesting a relatively high quantum yield of Mn^{2+} transition emission (4.6%, rhodamine B as reference). MnD ZnS QDs is one kind of the most interesting nanometer luminescent materials, which can emit weak blue fluorescence and strong orange RTP while the spectrofluorometer setting as fluorescence and phosphorescence modes, respectively. The fluorescence and RTP emission curves are shown in Fig. 5. The fluorescence emission at 430 nm is ascribed to a defect-related emission [19,24] and disappears in the phosphorescence mode. The observed orange emission at 580 nm (both RTP and fluorescence modes) is known to originate from the $^4T_1$ to $^6A_1$ transition of Mn^{2+} impurities incorporated into the ZnS host lattice excited via energy transfer from the ZnS host [15]. The phosphorescence lifetime of 2 ms for the synthesized AF MnD ZnS QDs was evaluated from the decay curve of its phosphorescence emission (see Inset (right) in Fig. 5).

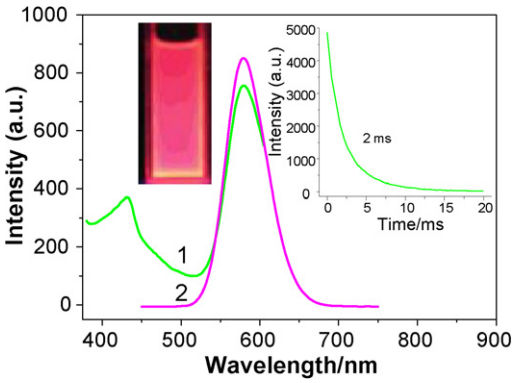

Fig. 5. Fluorescence (curve 1) and phosphorescence (curve 2) spectra of 400 mg/L AF MnD ZnS QDs aqueous solution. Insets are the photograph of 400 mg/L AF MnD ZnS QDs in a UV lamp box (left) and the decay curve of phosphorescence (right).

3.4. RTP and RLS spectra of TNT titrating AF MnD ZnS QDs

To explore the potential applications of the AF MnD ZnS QDs, the effects of TNT on the RTP and RLS spectra of the AF MnD ZnS QDs were investigated simultaneously. The results shown in Fig. 6A indicate that the $^4T_1$ to $^6A_1$ transition gradually reduced with the

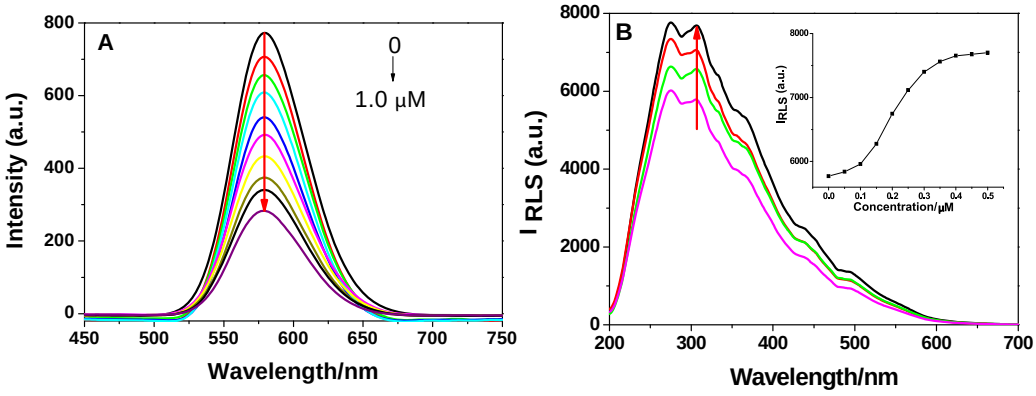

Fig. 6. TNT concentration-dependent phosphorescence (A) and RLS (B) spectra of the AF MnD ZnS QDs (10 μL of TNT stock solution was injected into QDs solution every time).

TNT being injected into the QDs aqueous solution. Compared with reported emission quenching [19,34], our AF MnD ZnS QDs probe held equivalent signal-amplified output which made the developed method also ultrasensitive in monitoring TNT analyte down to nanomolar levels (see Section 3.7). The signal change of RLS showed in Fig. 6B. RLS mechanism lies in non-homogeneous phase size effect caused by incorporation or polymerization of particles in system. With TNT being added into aqueous system, the RLS signal of AF MnD ZnS QDs became greater and greater, implying the interaction between AF MnD ZnS QDs and TNT.

3.5. Selectivity of the AF MnD ZnS QDs-based RTP method

The RTP quenching followed the Stern–Volmer equation showed in Eq. (1):

$$\frac{I_0}{I} = 1 + K_{SV}C_q \quad (1)$$

$$S_{OA} = K_{SV},\ \frac{T_{NT}}{K_{SV,OA}} \quad (2)$$

where I_0 and I are the phosphorescent intensities in the absence and presence of quenchers, respectively, C_q is the concentration of the quencher, OA represents other nitro aromatic compounds except for TNT, and K_{SV} is the quenching constant of the quenchers. The ratio (S) of K_{SV} of TNT and other analytes was adopted to evaluate the selectivity of the materials. The same measurement process replicated three times. The results were shown in Fig. 7A. The K_{SV} value for TNT, DNT, NT and 4-NP is 1.138, 0.451, 0.263 and 0.116, respectively. The corresponding S_{DNT}, S_{NT} and $S_{4\text{-NP}}$ value is 2.52, 4.33 and 9.78, respectively, which indicated that our luminescent probe possesses excellent selectivity for TNT, and therefore can sense TNT in environmental and biological samples ultraselectively without the interferences from other nitro aromatic compounds. The electron-deficient nitroaromatic species can be absorbed onto the surface of electron-rich ligands-capped nanocrystals. Therefore, the amine-capped nanocrystals have a stronger affinity to nitroaromatic species than MnD ZnS QDs@SiO_2 nanocrystals, leading to a higher quenching ratio of Mn transition emission at same concentration of nitroaromatic species. Moreover, the resultant anion species may increase the charge-transfer pathways from the nanocrystals to nitroaromatic analytes, therefore further enhance the quenching efficiency of phosphorescence. Fig. 7B shows the Stern–Volmer curves of nitroaromatic and nitrophenol species titrating MnD ZnS QDs@SiO_2 nanocrystals. The K_{SV} value for TNT, DNT, NT and 4-NP are 0.293, 0.191, 0.138 and 0.09, respectively. Which are 0.258, 0.424, 0.523 and 0.781-fold those for AF MnD ZnS QDs, respectively. The above results indicated the APTES as capped reagents can enlarge the spectral sensitivity and enhance phosphorescence response of nanocrystals to the electron-deficient nitroaromatic and nitrophenol species.

To learn the high selectivity of the present probe for TNT, the UV–vis spectra and colorimetric visualization were also performed in order to investigate the interaction of APTES with TNT. As shown in Fig. 2, while APTES was injected into TNT ethanol solution, new absorption bands was observed, the peak absorption lay in 465 nm, 525 nm and weaker band ranged from 600 to 700 nm, and the absorption peak gradually increased with the persistent addition of APTES, which implied the generation of third phase in solution, namely, the formation of TNT anion. Meanwhile, the photographs of APTES titrating the TNT ethanol solution were taken and displayed the change of system color before and after the addition of TNT (see Inset in Fig. 2). To clarify the selectivity of APTES for TNT over other nitro aromatic compounds, such as DNT, NT and 4-NP, the analogous experiments were also performed between APTES and these aromatic compounds. The change of system color happened at the injection of 20 μL APTES, with very strong absorption at 465 nm and 525 nm measured. Whereas, even the concentration of nitro aromatic compounds was high to 100 mM while containing 250 μL APTES, there were no new absorption bands between 450 nm and 800 nm, and no change of system color was observed. Therefore, APTES clearly exhibited excellent selectivity for TNT over DNT, NT and 4-NP.

3.6. Figures of merit of AF MnD ZnS QDs-based RTP probe

The AF MnD ZnS nanocrystals display a relatively strong fluorescence brightness, and the amino ligands at the surface of nanocrystals have a high affinity to TNT molecules. Thus it can be expected the nanocrystal sensor to detect the ultratrace TNT analyte in solution. The concentration of the AF MnD ZnS nanocrystals about 400 mg/L was used to evaluate the lowest detection ability toward TNT through the addition of TNT into solution containing probe causing the detectable decrease in fluorescence intensity. A 50 nM TNT in AF MnD ZnS QDs aqueous solution was detected as 8% decrease in the fluorescence intensity (three replicate detection). In general, about 5% decrease in fluorescence intensity is used as a detectable standard as in fluorescence method. Therefore, the low detection limit of the TNT analyte testified that the AF MnD ZnS nanocrystals have a strong enriching effect to the ultratrace TNT in solution, and the resultant TNT anions have a high quenching ability to the Mn^{2+} transition emission.

The AF MnD ZnS QDs have distinct linearly RTP quenching toward TNT in the concentration range of 0.05–1.8 μM with a correlation coefficient of 0.9902 and a linear regression equation of $\Delta I = 650.23C + 37.31$ (where C is the concentration of TNT in μM, ΔI is the error of original with instant phosphorescence intensity). The

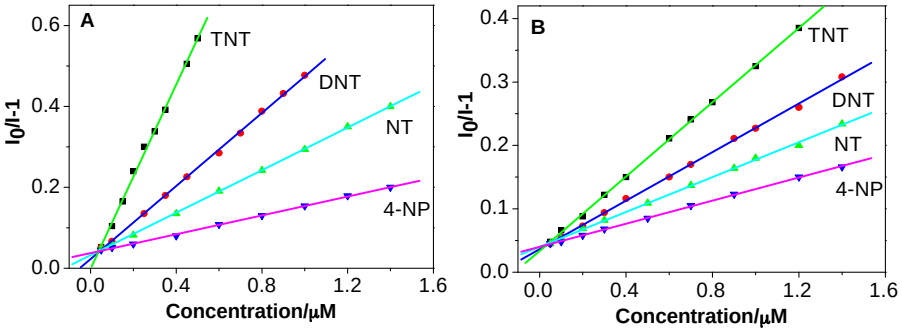

Fig. 7. Demonstrating selectivity of AF MnD ZnS QDs (A) and MnD ZnS QDs@SiO_2 (B) probes for TNT over other nitro aromatic compounds.

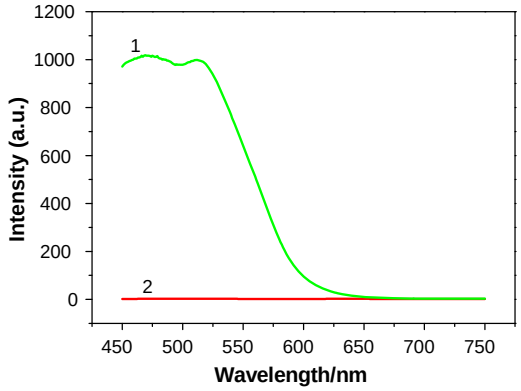

Fig. 8. Fluorescence (curve 1) and phosphorescence (curve 2) spectra of real rivers or lakes water matrix.

precision for five replicate detections of 0.1 μM TNT was 3.5% (RSD). Even though RTP-based analytical method is a method featuring much evident advantages and disadvantages, the most important advantage of RTP over fluorescence, the avoidance of the interference from autofluorescence and scattering light, was expected for the analysis of complex biological and environmental samples in order to lessen tedious sample pretreatment procedures.

3.7. Application of the AF MnD ZnS QDs for RTP sensing TNT in aqueous solution

The proposed AF MnD ZnS QDs-based RTP method was applied to determine TNT in local rivers and lakes water samples. The difference in the background of a real water matrix were shown in Fig. 8 while the detection modes being set as fluorescence and phosphorescence. No RTP but significant fluorescent background was observed for the real water sample. Such fluorescent background may result from the fluorescent matrix or scattering light of the samples [21]. Moreover, this RTP sensor gave excellent selectivity for detecting TNT in the presence of metal ions and organic compounds in real water sample. Quenching of the RTP due to the addition of TNT at 0.1 μM was unaffected by 1000-fold excesses of Li^+ (0.102 mg/L), Na^+ (14.53 mg/L), K^+ (3.667 mg/L), Mg^{2+} (0.221 mg/L), Ca^{2+} (25.12 mg/L), Sr^{2+} (0.095 mg/L) and Al^{3+} (0.023 mg/L) (the data in bracket represent their real concentration). Fulvic acid as the representative of organic compounds was permitted at saturated solution of pH 7.5, without interference with the detection of TNT. The quantitative recoveries were 105.8%, 102% and 96.5%, respectively, for the rivers and lakes water spiked with 50, 75 and 100 nM TNT. To demonstrate the potential utility of the present method for real samples, two river water samples spiked by mixtures of TNT, DNT, NT and 4-NP with different concentration, that is, 0.1, 1.0, 1.0, 1.0 μM and 0.3, 2.0, 2.0, 2.0 μM, respectively, were also analyzed for TNT. The concentrations of TNT in the spiked river samples determined by the proposed method were in good agreement with those of added TNT (determined results are 0.103 ± 0.01 and 0.32 ± 0.02, respectively), along with the quantitative recovery 103% and 106%, demonstrating the potential applicability of AF MnD ZnS QDs for the determination of TNT in real samples.

4. Conclusions

In summary, AF MnD ZnS QDs were prepared to be firsyly through the use of silane coupling agents to form an active layer of silica, then sol–gel reaction of TEOS co-deposited with APTES on the surface of resultant MPTS capped MnD ZnS QDs. The developed AF MnD ZnS QDs-based RTP quenching methods can simply, sensitively, and selectively detect ultratrace TNT in water. Although the research on nanocrystal-based RTP chemosensor is in its infancy, the obtained results confirmed the possibility without tedious sample pretreatment procedures, implying a great potential for the design and synthesis of nanometer devices and machines for the analysis of complex biological and environmental samples. Endeavors to explore the application of RTP device are currently in progress.

References

[1] A. Guerrero-Martínez, J. Pérez-Juste, L.M. Liz-Marzán, Adv. Mater. 22 (2010) 1182.
[2] P. Yang, M. Ando, N. Murase, J. Colloid Interf. Sci. 316 (2007) 420.
[3] M. Ohmori, E. Matijevic, J. Colloid Interf. Sci. 160 (1993) 288.
[4] L.M. Liz-Marzán, A.P. Philipse, J. Colloid Interf. Sci. 176 (1995) 459.
[5] E.P. Plueddermann, Silane Coupling Agents, Plenum Press, New York, USA, 1991.
[6] L.M. Liz-Marzán, M. Giersig, P. Mulvaney, Chem. Commun. 6 (1996) 731.
[7] L.M. Liz-Marzán, M. Giersig, P. Mulvaney, Langmuir 12 (1996) 4329.
[8] D.K. Yi, S.T. Selvan, S.S. Lee, G.C. Papaefthymiou, D. Kundaliya, J.Y. Ying, J. Am. Chem. Soc. 127 (2005) 4990.
[9] Z. Zhelev, H. Ohba, R. Bakalova, J. Am. Chem. Soc. 128 (2006) 6324.
[10] Y. Piao, A. Burns, J. Kim, U. Wiesner, T. Hyeon, Adv. Funct. Mater. 18 (2008) 1.
[11] Y. Yang, L. Jing, X. Yu, D. Yan, M. Gao, Chem. Mater. 19 (2007) 4123.
[12] M. Darbandi, R. Thomann, Th. Nann, Chem. Mater. 17 (2005) 5720.
[13] I. Sánchez-Barragán, J.M. Costa-Fernández, M. Valledor, J.C. Campo, A. Sanz-Medel, Trends Anal. Chem. 25 (2006) 958.
[14] C. de Mello Donegá, A.A. Bol, A. Meijerink, J. Lumin. 96 (2002) 87.
[15] J.H. Chung, C.S. Ah, D.J. Jang, J. Phys. Chem. B 105 (2001) 4128.
[16] B.C. Cheng, Z.G. Wang, Adv. Funct. Mater. 15 (2005) 1883.
[17] J.M. Costa-Fernández, R. Pereiro, A. Sanz-Medel, Trends Anal. Chem. 25 (2006) 207.
[18] R. Thakar, Y. Chen, P.T. Snee, Nano Lett. 7 (2007) 3429.
[19] R. Tu, B. Liu, Z. Wang, D. Gao, F. Wang, Q. Fang, Z. Zhang, Anal. Chem. 80 (2008) 3458.
[20] Y. He, H.F. Wang, X.P. Yan, Chem. Eur. J. 15 (2009) 5436.
[21] H.F. Wang, Y. He, T.R. Ji, X.P. Yan, Anal. Chem. 81 (2009) 1615.
[22] Y. He, H.F. Wang, X.P. Yan, Anal. Chem. 80 (2008) 3832.
[23] P. Wu, Y. He, H.F. Wang, X.P. Yan, Anal. Chem. 82 (2010) 1427.
[24] W.-S. Zou, D. Sheng, X. Ge, J.-Q. Qiao, H.-Z. Lian, Anal. Chem. 83 (2011) 30.
[25] S. Nieto, A. Santana, S.P. Hernández, R. Lareau, R.T. Chamberlain, M.E. Castro, Proc. SPIE-Int. Soc. Opt. Eng. 5403 (2004) 256.

[26] K.C. Crellin, M. Widmer, J.L. Beauchamp, Anal. Chem. 69 (1997) 1092.
[27] K.S. Ro, A. Venugopal, D.D. Adrian, D. Constant, K. Qaisi, K.T. Valsaraj, L.J. Thibodeaux, D. Roy, J. Chem. Eng. Data 41 (1996) 758.
[28] R.C. Stringer, S. Gangopadhyay, S.A. Grant, Anal. Chem. 82 (2010) 4015.
[29] S.S.R. Dasary, A.K. Singh, D. Senapati, H. Yu, P.C. Ray, J. Am. Chem. Soc. 131 (2009) 13806.
[30] Y. Jiang, H. Zhao, N. Zhu, Y. Lin, P. Yu, L. Mao, Angew. Chem. Int. Ed. 47 (2008) 8601.
[31] D. Roeseling, T. Tuercke, H. Krause, S. Loebbecke, Org. Process. Res. Dev. 13 (2009) 1007.
[32] S. Kang, J.P. Green, Proc. Natl. Acad. Sci. U.S.A. 67 (1970) 62.
[33] J.V. Janovsky, L. Erb, Ber. Dtsch. Chem. Ges. 18 (1886) 2155.
[34] D. Gao, Z. Zhang, M. Wu, C. Xie, G. Guan, D. Wang, J. Am. Chem. Soc. 129 (2007) 7859.
[35] N.A. Al-Hashimi, Spectrochim. Acta A 60 (2004) 2181.